The Journal of Immunology

Prostaglandin E_2 Induces Oncostatin M Expression in Human Chronic Wound Macrophages through Axl Receptor Tyrosine Kinase Pathway

Kasturi Ganesh, Amitava Das, Ryan Dickerson, Savita Khanna, Narasimham L. Parinandi, Gayle M. Gordillo, Chandan K. Sen and Sashwati Roy

J Immunol 2012; 189:2563-2573; Prepublished online 27 July 2012;
doi: 10.4049/jimmunol.1102762
http://www.jimmunol.org/content/189/5/2563

The Journal of Immunology is published twice each month by
The American Association of Immunologists, Inc.,
1451 Rockville Pike, Suite 650, Rockville, MD 20852

Print ISSN: 0022-1767 Online ISSN: 1550-6606.

Prostaglandin E_2 Induces Oncostatin M Expression in Human Chronic Wound Macrophages through Axl Receptor Tyrosine Kinase Pathway

Kasturi Ganesh,* Amitava Das,* Ryan Dickerson,* Savita Khanna,* Narasimham L. Parinandi,† Gayle M. Gordillo,‡ Chandan K. Sen,* and Sashwati Roy*

Monocytes and macrophages (mϕ) are plastic cells whose functions are governed by microenvironmental cues. Wound fluid bathing the wound tissue reflects the wound microenvironment. Current literature on wound inflammation is primarily based on the study of blood monocyte-derived macrophages, cells that have never been exposed to the wound microenvironment. We sought to compare pair-matched monocyte-derived macrophages with mϕ isolated from chronic wounds of patients. Oncostatin M (OSM) was differentially overexpressed in pair-matched wound mϕ. Both PGE_2 and its metabolite 13,14-dihydro-15-keto-PGE_2 (PGE-M) were abundant in wound fluid and induced OSM in wound-site mϕ. Consistently, induction of OSM mRNA was observed in mϕ isolated from PGE_2-enriched polyvinyl alcohol sponges implanted in murine wounds. Treatment of human THP-1 cell-derived mϕ with PGE_2 or PGE-M caused dose-dependent induction of OSM. Characterization of the signal transduction pathways demonstrated the involvement of EP4 receptor and cAMP signaling. In human mϕ, PGE_2 phosphorylated Axl, a receptor tyrosine kinase (RTK). Axl phosphorylation was also induced by a cAMP analogue demonstrating interplay between the cAMP and RTK pathways. PGE_2-dependent Axl phosphorylation led to AP-1 transactivation, which is directly implicated in inducible expression of OSM. Treatment of human mϕ or mice excisional wounds with recombinant OSM resulted in an anti-inflammatory response as manifested by attenuated expression of endotoxin-induced TNF-α and IL-1β. OSM treatment also improved wound closure during the early inflammatory phase of healing. In summary, this work recognizes PGE_2 in the wound fluid as a potent inducer of mϕ OSM, a cytokine with an anti-inflammatory role in cutaneous wound healing. ***The Journal of Immunology*****, 2012, 189: 2563–2573.**

In the United States, chronic wounds affect 6.5 million patients, thus posing a major threat to the public health and economy (1). Yet, studies directly investigating chronic wounds as presented in the clinic to develop mechanism-based understanding are scanty. Macrophages (mϕ) play a key role in wound repair such that both inadequate inflammatory responses to wounding and unresolved inflammation compromise wound closure (2, 3). Monocytes are highly plastic cells that differentiate into mϕ based on cues at the specific wound microenvironment (4). The functional fate of monocytes recruited to the wound site is governed by the specific properties of the wound microenvironment (4, 5). We recognize that peripheral blood monocytes differentiated ex vivo using standard laboratory procedures do form mϕ but do not resemble wound mϕ because of the lack of exposure to an elaborate set of microenvironmental cues ex vivo. Wound mϕ can thus only be studied functionally if they can be isolated intact from the actual wound milieu. Characterization of the phenotype of wound mϕ obtained using the polyvinyl alcohol (PVA) sponge approach led to the recognition that wound mϕ possess unique characteristic features (6, 7). At present, evidence supporting the understanding of mϕ directly isolated from the human wound milieu is scanty. Thus, we sought to develop an approach to collect functionally intact mϕ from clinically presented chronic wounds. Outcomes from such cells were compared in a pair-matched manner with the peripheral blood monocyte-derived macrophages (MDM) of the same individual. Such studies identified oncostatin M (OSM) as a key cytokine that is differentially expressed and abundantly produced by human chronic wound mϕ. OSM is a multifunctional cytokine known to be produced by activated mϕ. It is structurally and functionally related to the IL-6 type cytokine family (8–10). In this work, we sought to characterize the mechanism underlying OSM induction in wound mϕ and to understand the significance of OSM in wound inflammation.

Materials and Methods

Human subjects and sample collection

Subjects (n = 15) participating in the study were chronic wound patients seen at The Ohio State University Comprehensive Wound Center clinics and have been undergoing negative pressure wound therapy (NPWT) as

*Department of Surgery, Center for Regenerative Medicine and Cell-Based Therapies and Comprehensive Wound Center, Davis Heart and Lung Research Institute, The Ohio State University Wexner Medical Center, Columbus, OH 43210; †Department of Internal Medicine, Center for Regenerative Medicine and Cell-Based Therapies and Comprehensive Wound Center, Davis Heart and Lung Research Institute, The Ohio State University Wexner Medical Center, Columbus, OH 43210; and ‡Department of Plastic Surgery, Center for Regenerative Medicine and Cell-Based Therapies and Comprehensive Wound Center, Davis Heart and Lung Research Institute, The Ohio State University Wexner Medical Center, Columbus, OH 43210

Received for publication September 29, 2011. Accepted for publication June 20, 2012.

This work was supported by National Institute of Diabetes and Digestive and Kidney Diseases Grant R01 DK076566 (to S.R.) and by National Institute of General Medical Sciences Grants GM069589 and GM077185 (to C.K.S.) and GM095657 (to G.M.G.).

Address correspondence and reprint requests to Dr. Sashwati Roy, The Ohio State University Wexner Medical Center, 473 West 12th Avenue, 511 Davis Heart and Lung Research Institute, Columbus, OH 43210. E-mail address: sashwati.roy@osumc.edu

Abbreviations used in this article: BMDM, bone marrow-derived macrophage; db-cAMP, dibutyryl cyclic AMP; mϕ, macrophage; MDM, monocyte-derived macrophage; NPWT, negative pressure wound therapy; OSM, oncostatin M; PGE-M, 13,14-dihydro-15-keto-PGE_2; PVA, polyvinyl alcohol; qPCR, quantitative PCR; RTK, receptor tyrosine kinase; siRNA, small interfering RNA.

www.jimmunol.org/cgi/doi/10.4049/jimmunol.1102762

part of standard clinical care. Demographic characteristics of patients and wound-related information are presented in Table I. The NPWT dressing (sponges) and peripheral blood were collected from each patient. All human studies were approved by The Ohio State University Institutional Review Board. Declaration of Helsinki protocols was followed, and patients gave their written informed consent.

Human chronic wound macrophage and fluid collection

Wound fluid and cells were derived from the NPWT dressing by lavaging the wound dressing with saline solution (11). The lavaged fluid was centrifuged to obtain wound cells. Wound mϕ were isolated from NPWT sponge-derived wound cells using Ficoll density centrifugation followed by MACS (Miltenyi Biotec, Auburn, CA) using CD14 Ab. Isolated cells were seeded in culture dishes for 3 h. Nonadherent cells were washed and removed. The phenotype of adherent cells was confirmed by immunofluorescence staining using CD68 Ab.

Peripheral blood MDM

Blood monocytes from human subjects were isolated using a Ficoll-Hypaque density gradient (GE Healthcare [formerly Amersham Biosciences], Piscataway, NJ). Positive selection for monocytes was performed using CD14 Ab conjugated to magnetic beads (Miltenyi Biotec). Purity of these preparations of monocytes was >90% as determined by FACS analyses using CD14 Abs. Differentiation of these cells to mϕ was performed as described (11).

Isolation of murine wound mϕ and bone marrow-derived macrophages

For wound mϕ, circular (6 mm) sterile PVA sponges were implanted s.c. on the backs of 8- to 10-wk-old C57Bl/6 mice. Sponge-infiltrated mϕ were isolated as described (12). To obtain bone marrow-derived macrophages (BMDM), the cells from femurs of mice (9 wk old) were flushed using RPMI 1640 followed by positive selection using CD11b Ab conjugated to magnetic beads. The isolated cells were cultured in RPMI 1640 containing 10% heat-inactivated FBS, 1% antibiotic/antimycotic, polymyxin B (10 μg/ml), and mouse MCSF (20 ng/ml) at 37˚C in a humidified atmosphere containing 5% CO_2 for 5 d (13, 14).

"Hunt–Schilling" wire mesh cylinder for wound fluid collection

The implantation of wire mesh cylinders (stainless steel; 2.5-cm length and 0.8-cm diameter) and wound fluid harvest was performed as described previously (15). After anesthesia, midline incision (1 cm or smaller) was made on shaved skin with a scalpel. Small s.c. pockets were created by blunt dissection. Two wire mesh stainless steel cylinders were inserted into each pocket. Sutures and staples were used to close the incisions. After 3 d of implantation, wound fluid was harvested for analysis.

Secondary-intention excisional dermal splinted murine wound model

Contraction of excisional murine wounds was limited by the application on a split so that the wound could heal through the processes of granulation and re-epithelialization (16). After anesthesia applied as isoflurane inhalation, two 6-mm full-thickness (skin and panniculus carnosus) excisional wounds were placed on the dorsal skin (shaved and cleaned using Betadine), equidistant from the midline and adjacent to the four limbs. A donut-shaped splint with an 8-mm inner diameter created from an 0.5-mm-thick silicone sheet (Grace Bio-Laboratories, Bend, OR) was placed such that the wound was centered within the splint. To affix the splint to the skin, an immediate-bonding adhesive was used followed by interrupted 6-0 nylon sutures (Ethicon, Somerville, NJ). The wound was covered with semiocclusive dressing (Tegaderm; 3M, St. Paul, MN). Recombinant mouse OSM was injected under the Tegaderm as needed. All animal studies were approved by The Ohio State University Institutional Animal Care and Use Committee.

Determination of wound area

The imaging of wounds was performed using a digital camera (Canon PowerShot G6). The wound area was determined by planimetry using ImageJ software as described (17).

GeneChip probe array analyses

RNA extraction, target labeling, and GeneChip and data analyses were performed as described previously (17–20). In brief, GeneChip IVT Labeling Kit (Affymetrix, Santa Clara, CA) in vitro transcription reaction was used to generate biotinylated cRNA from RNA samples. The samples were hybridized to Affymetrix Human Genome U133 Plus 2.0 Array. The arrays were washed, stained with streptavidin–PE, and scanned with the GeneArray scanner (Affymetrix) in our own facilities as described earlier (18, 19, 21, 22).

Data analyses

Data acquisition and image processing was performed using Gene Chip Operating Software (Affymetrix). The expression data have been submitted to the Gene Expression Omnibus database (http://www.ncbi.nlm.nih.gov/geo) under the series accession number GSE36995. Raw data were analyzed using Genespring GX (Agilent, Santa Clara, CA). Additional processing of data was performed using dChip software (Harvard University) (18, 19, 21, 22).

ELISA

Levels of OSM (R&D Systems, Minneapolis, MN), PGE_2, and 13,14-dihydro-15-keto-PGE_2 (PGE-M; Cayman Chemicals, Ann Arbor, MI) in wound fluid were measured using commercially available ELISA kits. The levels of OSM, PGE_2, and PGE-M in wound fluid were normalized against albumin concentration in the fluid. Albumin levels were determined by ELISA (AssayPro, St. Charles, MO). For measurement of OSM produced by mϕ, cells were seeded in 6-well or 12-well plates and cultured in RPMI 1640 medium containing 10% heat-inactivated bovine serum for 24 h under standard culture conditions. After 24 h, the culture media was collected, and OSM levels were measured using ELISA as described. Phospho-Axl, total Axl, and cAMP levels were measured from cell lysates using a sandwich ELISA (R&D Systems).

Reverse transcription and quantitative RT-PCR

Total RNA was extracted using the mirVana RNA isolation kit (Ambion, Austin, TX) according to the manufacturer's instructions. mRNA was quantified by real-time or quantitative PCR (qPCR) assay using the dsDNA binding dye SYBR Green-I as described previously (17, 20).

Phospho-receptor tyrosine kinase array

Receptor tyrosine kinase (RTK) Ab arrays were purchased from R&D Systems (no. ARY-001). Cell harvest, sample preparation, and RTK array assay were performed as recommended by the manufacturer (11).

Small interfering RNA delivery

DharmaFECT (Dharmacon RNA Technologies, Lafayette, CO) was used to transfect cells with a 100 nM small interfering RNA (siRNA) pool (Dharmacon RNA Technologies) for 48 h as described (23). For control, siControl nontargeting siRNA pool (mixture of four siRNAs, designed to have ≥4 mismatches with the gene) was used.

Analysis of specific binding of AP-1 to DNA

Nuclear protein extracts of cells were prepared using the nuclear extract kit (Active Motif, Carlsbad, CA) according to the manufacturer's instructions. Binding of Fos and Jun family proteins to their consensus sites was determined using a ELISA-based Trans-AM AP-1 kit (Active Motif, Carlsbad, CA).

Statistics

In vitro data are reported as mean ± SD of three to six experiments as indicated in the respective figure legends. Comparisons among multiple groups were tested using ANOVA, and $p < 0.05$ was considered statistically significant. For animal studies, data are reported as mean ± SD of at least three to four animals as indicated. Given the small sample size, Mann–Whitney or Kruskal–Wallis one-way ANOVA test was performed to test significance ($p < 0.05$) of difference between means. For wound fluid studies, data from 15 human subjects ($n = 15$) are presented (Table I).

Results

This work developed a novel approach to isolate and culture functionally intact mϕ from chronic wounds of human subjects (Table I). To compare the wound mϕ with corresponding mϕ derived from peripheral blood monocytes (i.e., MDM), transcriptome profiling (GeneChip Affymetrix) was performed. OSM was among the top-ranked differentially expressed genes that were highly upregulated in wound mϕ compared with MDM. An ~9-fold induction in the expression of OSM was observed in wound mϕ compared with pair-

Table I. Demographic characteristics of patients (n = 15) and wound size and age

Age (y)	47 ± 8
Female	8
Race	African American, White
Wound size (mm^3)	4.5–729
Wound age	>30 d
Diabetic	8
Wound cause	
Pressure	7
Surgical	8
Wound location	
Abdominal	5
Lower extremity	10

matched blood-derived MDM of the same individual (Fig. 1A). To test the validity of OSM outcomes as evident in profiling data, wound mϕ and MDM were isolated from patients and cultured overnight. Consistent with GeneChip data, the level of OSM protein released by wound mϕ was multifold higher (~3-fold) compared with that released by peripheral blood MDM of the same individual (Fig. 1B). Consistent with elevated production of OSM by cultured wound mϕ, wound fluid derived from chronic wounds contained elevated levels of OSM compared with those of pair-matched blood plasma samples from the same patients (Fig. 1C). PGE_2 is a known inducer of OSM expression in mϕ (24). High levels of PGE_2 were noted in wound fluids compared with those of pair-matched blood plasma obtained from chronic wound patients (Fig. 1D). In vivo, PGE_2 is rapidly metabolized to PGE-M (25). A higher level of PGE-M was also detected in wound fluid compared with that in matched plasma samples (Fig. 1E). Plasma levels of PGE-M in humans are known to be in the range of 10–100 pg/ml (25). We detected ~20-fold higher levels of PGE-M in wound fluid obtained from chronic wounds compared with those of matched plasma (Fig. 1E). Of interest in this context is the observation that OSM may induce PGE_2 (26). In the wound microenvironment, PGE_2 may be contributed by a number of cells including mϕ (27). To test whether wound mϕ produce PGE_2, levels of this eicosanoid were measured in wound mϕ culture media. Multifold higher levels of PGE_2 were detected in such culture media compared with those of media hosting MDM (Fig. 1F). This observation recognizes wound mϕ as a direct source of PGE_2 in the wound microenvironment.

To characterize the mechanism of PGE_2-induced OSM expression, human monocytic THP-1 cells were used. THP-1 cells were differentiated to mϕ using PMA (20 ng/ml, 48 h). PGE_2 dose-dependently induced OSM protein expression (Fig. 2A). After PGE_2 treatment, OSM gene and protein were significantly unregulated at 6 and 24 h posttreatment, respectively (Fig. 2B, 2C). In addition to PGE_2, PGE-M also induced OSM expression in a dose-dependent manner (Fig. 2D). The expression of OSM mRNA peaked at 48 h posttreatment (Fig. 2E). Consistent with findings using THP-1, PGE_2 potently induced OSM in MDM demonstrating that the finding is applicable to cells of monocytic lineage (Fig. 2F). PGE_2 is known to signal via G-protein–coupled receptors designated as EP1, EP2, EP3, and EP4 (28). To delineate the PGE_2-inducible signaling pathway that causes OSM expression in mature mϕ, EP receptors were screened for involvement. In mature mϕ, EP4 represented the most abundant EP receptor (Fig. 3A). Next, we addressed the significance of EP4 in PGE_2-induced OSM expression. Both inhibition of EP4 using the pharmacologic inhibitor L-161,982 (29) and knockdown of EP4 expression inhibited PGE_2-induced OSM expression (Fig. 3B, 3C). Transfection of cells with EP4 siRNA was successful in achieving ~70% knockdown of EP4 mRNA expression (Fig. 3D).

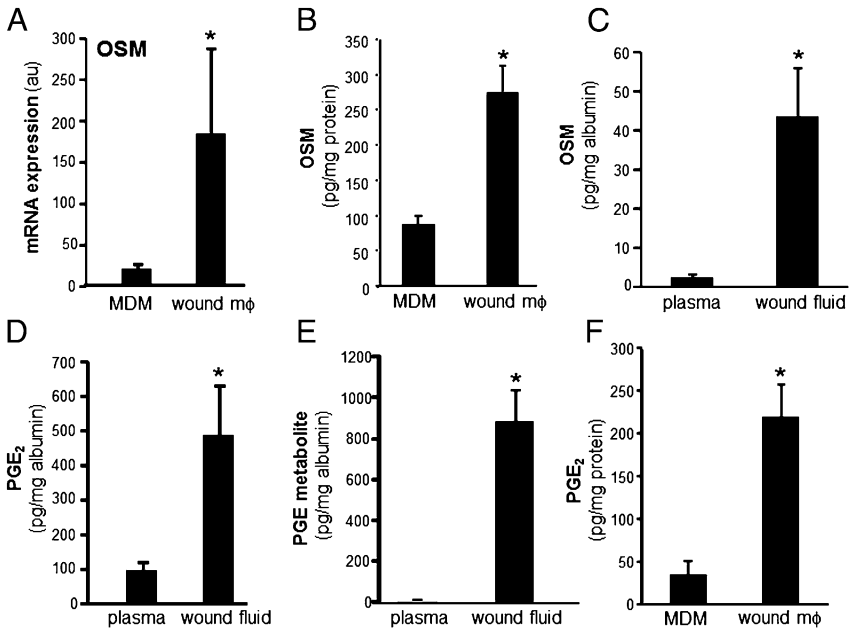

FIGURE 1. OSM as one of the highly expressed genes in mϕ from human chronic wounds. Wound site mϕ (wound mϕ) were isolated from human subjects with chronic wounds. Matching blood MDM were obtained as described in *Materials and Methods* from the same subjects. (**A**) Expression levels of OSM gene using GeneChip analysis. GeneChip expression values were normalized using global scaling approach. n = 3. *$p < 0.05$ (compared with matched MDM). (**B**) OSM expression data from GeneChip analysis was independently verified using ELISA. Wound site mϕ and matching MDM were cultured for 24 h. OSM released by the cells in media was measured by ELISA. n = 3. *$p < 0.05$ (matched MDM). (**C**–**E**) OSM, PGE_2, and its metabolite PGE-M are abundant in fluid from human chronic wounds. Fluid was obtained from chronic wounds of human subjects. The levels of (C) OSM, (D) PGE_2, and (E) PGE-M were determined using ELISA from chronic human wound fluid and matching plasma samples from the patients. The levels were normalized to the total albumin level in the fluid/plasma. n = 15. *$p < 0.01$ (compared with plasma). (**F**) Wound site mϕ and matching MDM were cultured for 24 h. PGE_2 released by the cells was measured in culture media using ELISA. n = 3. *$p < 0.05$ (matched MDM).

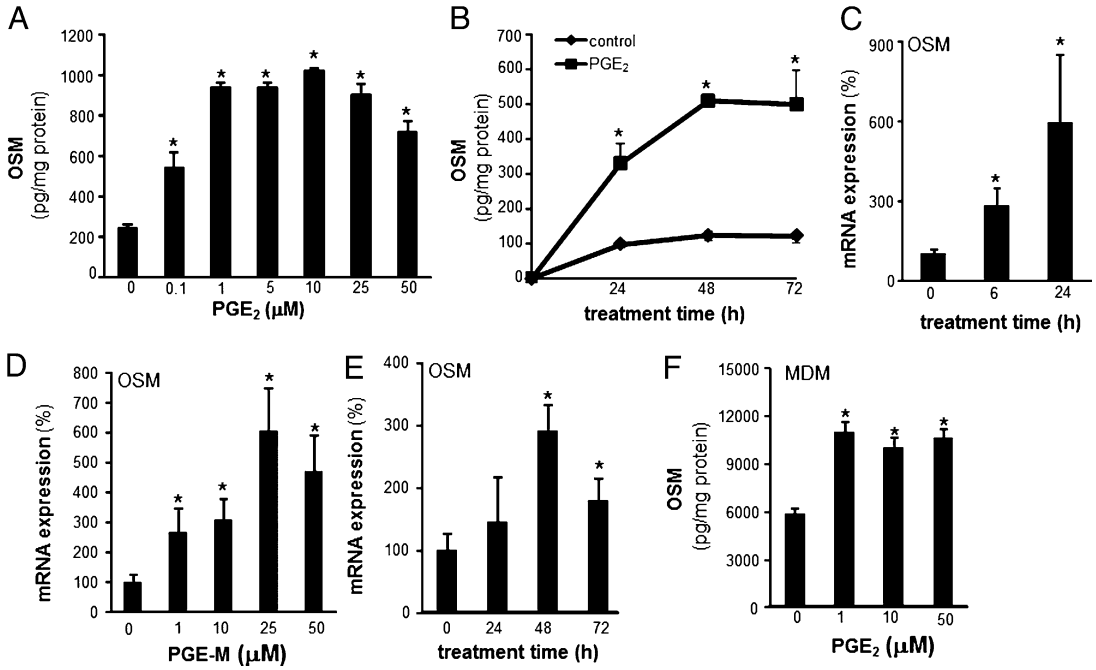

FIGURE 2. PGE$_2$ and PGE-M induced OSM gene and protein expression in human mϕ. Cells of the human monocytic cell line THP-1 were differentiated to mϕ with PMA (20 ng/ml, 48 h). (**A**) Cells were treated with a range of PGE$_2$ concentrations (0.1–50 μM). OSM level in media was measured after 72 h of treatment. Data are mean ± SD. (n = 5). *$p < 0.05$ (compared with control). (**B**) Cells were treated with PGE$_2$ (10 μm) for 0–72 h. OSM protein in media was measured using ELISA. OSM levels were normalized to total cellular protein in the culture. Data are mean ± SD (n = 4). *$p < 0.05$ (compared with control). (**C**) Cells were treated with PGE$_2$ (10 μm) for 0–24 h. OSM gene expression was measured using qPCR. Data are mean ± SD (n = 4). *$p < 0.05$ (compared with control). (**D**) Cells were treated with varying concentrations (1–50 μM) of PGE-M for 72 h. OSM gene expression was measured using qPCR. Data are mean ± SD (n = 4). *$p < 0.05$ (compared with 0 μM). (**E**) Cells were treated with PGE-M (25 μm) for 0–72 h. OSM mRNA expression was measured. Data are mean ± SD (n = 4).*$p < 0.05$ (compared with 0 h). (**F**) MDM were treated with a range of PGE$_2$ concentrations (0.1–50 μM). OSM level in media was measured after 72 h of treatment. Data are mean ± SD (n = 5). *$p < 0.05$ (compared with control).

Activation of EP4 is known to induce intracellular cAMP as second messenger (30). We observed that PGE$_2$ rapidly and significantly induced cAMP levels in MDM (Fig. 4A). Studies testing the plausible involvement of EP2 in mediating PGE$_2$ signaling demonstrated that selective activation of the EP2 receptor using butaprost does not elevate cellular cAMP in MDM (Fig. 4A) arguing against the potential involvement of EP2 receptors in PGE$_2$-induced cAMP signaling. It may thus be concluded that abundantly expressed EP4 and not EP2 is the key receptor involved in PGE$_2$ signaling in MDM. We observed that the cAMP analogue dibutyryl cyclic AMP (db-cAMP) was effective in inducing OSM expression in human mϕ (Fig. 4B). Furthermore, the adenylate cyclase agonist forskolin also induced OSM expression (Fig. 4B). These data collectively establish that EP4 receptor mediates PGE$_2$-induced OSM expression through adenylate cyclase and cAMP signaling.

Efforts further to characterize the pathways involved in PGE$_2$-induced OSM production led to the observation that the RTK inhibitor herbimycin A potently inhibited PGE$_2$-induced OSM expression (Fig. 4C). To investigate which specific RTKs are activated as a result of PGE$_2$ treatment, we used an Ab array that allows simultaneous assessment of the phosphorylation status of 42 RTKs (human phospho-RTK array, ARY001; R&D Systems). This approach led to the observation that PGE$_2$ rapidly (30 min) induces Axl phosphorylation (Fig. 5A). This finding was verified by sandwich ELISA using Abs against phospho-Axl and total Axl. As observed with RTK array screening, potent induction in phosphorylation of Axl was observed after 30 min of PGE$_2$ treatment (Fig. 5B). Consistently, PGE$_2$ induced Axl phosphorylation in MDM (Fig. 5C). Similar to PGE$_2$, treatment of cells with db-cAMP also resulted in phosphorylation of Axl suggesting that cAMP is sufficient to induce Axl phosphorylation. These data unveil an interesting cross talk between cAMP and RTK pathways. Knockdown of Axl inhibited PGE$_2$-induced OSM expression demonstrating that Axl is directly implicated in PGE$_2$-induced OSM expression (Fig. 5C–E).

AP-1 binding sites are present on the human OSM promoter (31). We observed that DNA binding activity of AP-1 was induced in nuclear extracts of PGE$_2$-treated cells. Maximal activation was observed after 1 h of PGE$_2$ treatment (Fig. 6A). The timeline of induction of RTK phosphorylation (30 min) and AP-1 DNA binding activity (60 min) suggested that phosphorylation of Axl is upstream to induction of AP-1 transactivation. Of the AP-1 proteins, FosB, JunD, and Fra-1 were observed to be not sensitive to PGE$_2$ treatment. However, cFos, cJun, and JunB were identified as PGE$_2$-sensitive AP-1 proteins (Fig. 6B–D). PGE$_2$-induced DNA binding activity of AP-1 was verified using a lower concentration (1 μM) of PGE$_2$ (Fig. 7A). PGE$_2$-induced activation of AP-1 was comparable to the activation by a classical phorbol ester inducer (PMA) (32) (Fig. 7B). Specific inhibition of Axl using R428 (SYN-1131; Synkinase) (33) significantly blunted PGE$_2$-mediated AP-1 activation (Fig. 7B). siRNA knockdown studies demonstrated that Axl specifically regulated PGE$_2$-induced activation of Jun (cJun and JunB) proteins (Fig. 7C, 7D), but not that of cFos (data not shown).

Consistent with the outcome of Axl knockdown studies, db-cAMP resulted in activation of cJun and JunB but not of cFos (Fig. 7E, 7F). Taken together, these findings indicate that PGE$_2$ elicits convergent RTK and cAMP signaling that culminates in OSM expression. To test whether PGE$_2$ may induce OSM production by wound mϕ in vivo, PVA sponges containing either

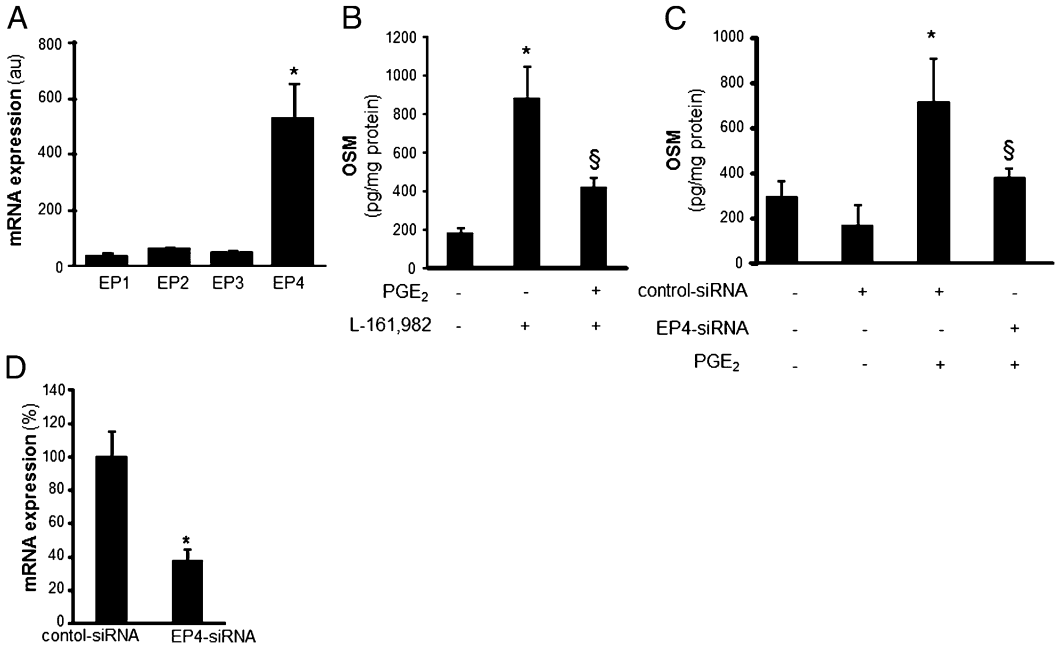

FIGURE 3. Role of PGE_2 receptor expression and function in PGE_2-induced OSM expression. (**A**) Relative expression of four PGE_2 receptors (EP1–EP4) in differentiated THP-1 mϕ. The mRNA expression of EP receptors was determined using qPCR. Data are mean ± SD ($n = 4$). *$p < 0.01$ (compared with EP1–EP3). (**B**) Cells were pretreated (1 h) with L-161,982 (EP4 antagonist, 100 nM) followed by treatment with PGE_2 (10 μM, 72 h). Level of OSM in culture media was measured using ELISA. Data are mean ± SD ($n = 6$). *$p < 0.01$ (compared with untreated cells), §$p < 0.05$ (compared with PGE_2-treated cells). (**C**) Cells were subjected to EP4 knockdown (EP4-siRNA) or not (control-siRNA). After 72 h of siRNA transfection, the cells were treated with PGE_2 (10 μM, 72 h). Level of OSM in culture media was measured using ELISA. Data are mean ± SD ($n = 3$). *$p < 0.01$ (compared with PGE_2 untreated cells), §$p < 0.05$ (compared with PGE_2-treated and control-siRNA–treated cells). (**D**) EP4 knockdown was achieved by transfection of cells with EP4-siRNA versus control-siRNA. EP4 mRNA levels were determined in cells using qPCR. Data are mean ± SD ($n = 3$). *$p < 0.05$ (compared with control).

PGE_2 or vehicle (ethanol) were s.c. implanted on the backs of C57BL/6 mice. Potent induction of OSM mRNA expression was observed in mϕ isolated from PVA sponges containing PGE_2 (2 nmol/sponge; Fig. 8A). Consistently, PGE_2 treatment also induced OSM production in human wound mϕ (Fig. 8B). Human wound mϕ demonstrated elevated expression of EP4 receptor (Fig. 8C). Exposure to PGE_2 resulted in increased phosphorylation of Axl in wound mϕ suggesting that the PGE_2-induced OSM pathway involves EP4–RTK signaling as observed in THP-1 cells (Fig. 8D, 8E). Next, the significance of wound fluid PGE_2 and cyclooxygenase-derived PGs in induction of wound mϕ OSM was determined. Treatment of MDM with culture media containing specific dilutions of sterile-filtered wound fluid potently induced OSM expression (Fig. 9A). Matching volume of human AB serum was added to the culture medium as a control for wound fluid. Treatment of wound fluid with anti-PGE_2 Ab resulted in sequestration of PGE_2 from wound fluid. To determine if such sequestration blocks biological activity of PGE_2, we determined whether wound fluid may induce cAMP levels and whether anti-PGE_2 treatment is able to block such effect. These data demonstrate that

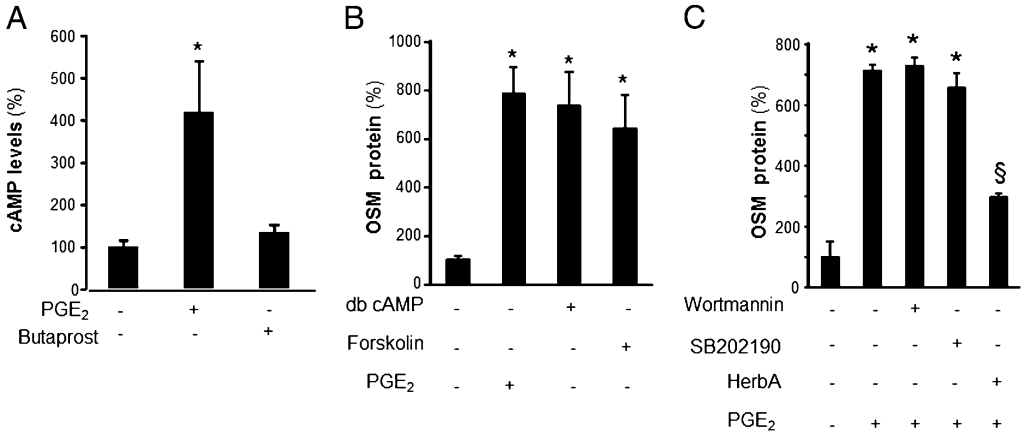

FIGURE 4. Adenylate cyclase, cAMP, and RTK are involved in PGE_2-induced OSM expression. (**A**) Blood MDM were treated with PGE_2 (1 μM) or butaprost (EP2 agonist, 1 μM) for 5 min. Cellular levels of cAMP were determined using ELISA. Data are mean ± SD ($n = 4$). *$p < 0.01$ (compared with untreated cells). (**B**) Differentiated human THP-1 mϕ were treated with an activator of adenylate cyclase, forskolin (100 μM), db-cAMP (100 μM), or PGE_2 (10 μM) for 72 h. (**C**) Cells were pretreated with SB202190 (5 μM), a p38 MAPK inhibitor, the PI3K inhibitor wortmannin (50 nM), or RTK inhibitor herbimycin A (5 μg/ml, HerbA) for 30 min followed by treatment with PGE_2 for 72 h. The level of OSM in culture media in both (B) and (C) was measured using ELISA. Data are mean ± SD ($n = 4$). *$p < 0.01$ (compared with untreated cells), §$p < 0.05$ (compared with PGE_2-treated cells).

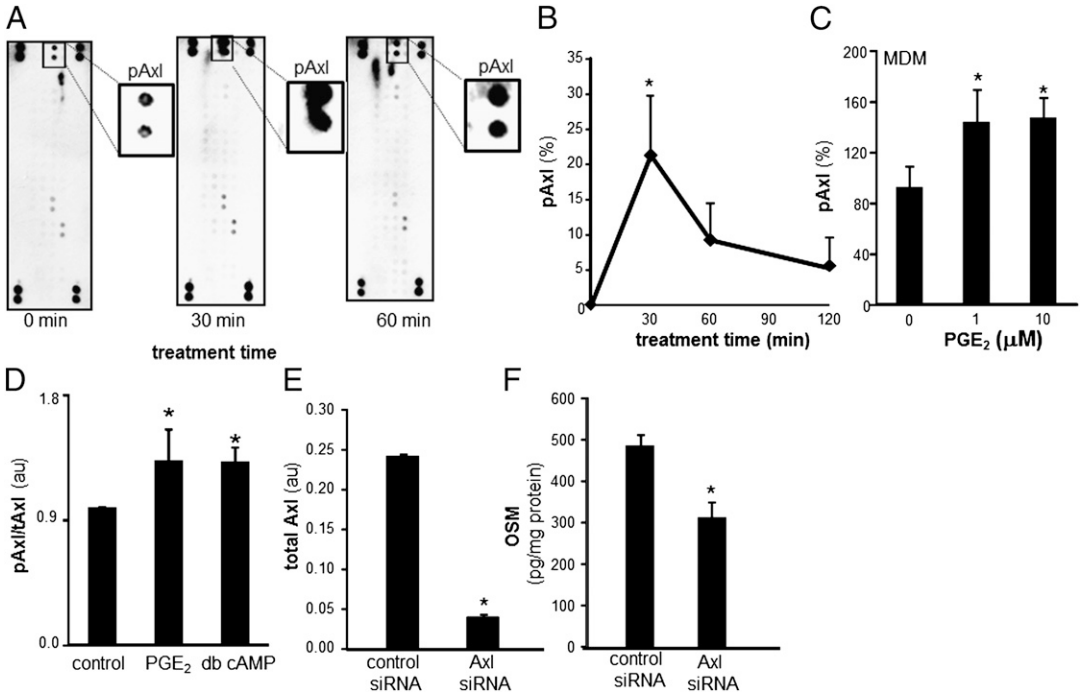

FIGURE 5. RTK Axl is phosphorylated after treatment of mϕ with PGE$_2$: involvement of Axl in regulation of PGE$_2$-mediated OSM production. (**A**) Differentiated human THP-1 mϕ were treated with PGE$_2$ (10 μM) for 30 and 60 min. Relative phosphorylation of 42 RTKs was screened using phospho-RTK array. The screening revealed PGE$_2$ specifically phosphorylates Axl (pAxl) after 30 min of PGE$_2$ treatment. Insets are zoomed images of pAxl spots in the array. (**B**) The array data were verified using sandwich ELISA to measure tyrosine-phosphorylated Axl in cell lysates. pAxl data were normalized against total Axl (tAxl) present in cell lysates. Data are expressed as percent change compared with time 0 h. Data are mean ± SD (n = 4). *$p < 0.05$ (compared with 0 h). (**C**) MDM were treated with PGE$_2$ (1–10 μM) for 30 min. ELISA was used to measure tyrosine-phosphorylated Axl in cell lysates. Data are mean ± SD (n = 3). *$p < 0.05$ (compared with control). (**D**) Differentiated human THP-1 mϕ were treated with PGE$_2$ (10 μM) and db-cAMP (100 μm) for 30 min. pAxl/tAxl levels were detected using sandwich ELISA. Data are mean ± SD (n = 4). *$p < 0.05$ (compared with control). (**E**) Axl knockdown was achieved by transfection of cells with Axl siRNA versus control siRNA. Total Axl levels were determined in cell lysates using ELISA. Data are mean ± SD (n = 3). *$p < 0.05$ (compared with control). (**F**) Axl knockdown cells were treated using PGE$_2$ (10 μM) for 72 h. The level of OSM in culture media was measured using ELISA. Data are mean ± SD (n = 4). *$p < 0.05$ (compared with control siRNA-transfected cells).

level as well as biological activity of PGE$_2$ was effectively blocked using anti-PGE$_2$ Ab (Fig. 9B, 9C). Such blockade of PGE$_2$ resulted in significant inhibition of wound fluid-induced OSM expression in MDM (Fig. 9D). Murine wound mϕ obtained from s.c. implanted PVA sponges showed higher expression of OSM mRNA compared with murine BMDM (Fig. 9E). Oral supplementation (gavage) of mice with indomethacin (1 mg/kg/d) or saline (control) for 5 consecutive days resulted in atten-

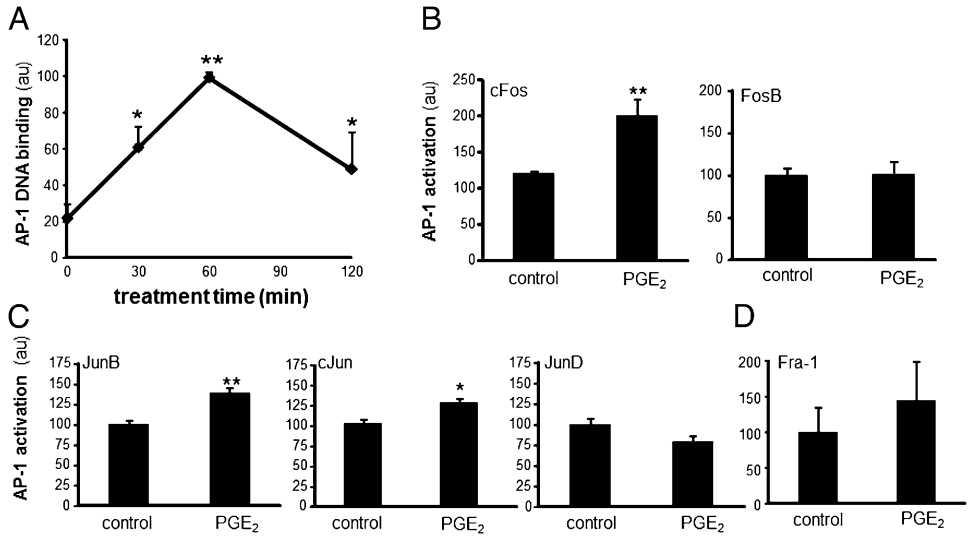

FIGURE 6. Induction of AP-1 DNA binding activity by PGE$_2$. (**A**) An ELISA-based (Trans-AM) method was used to analyze DNA binding activities of AP-1 from differentiated THP-1 mϕ treated with PGE$_2$ (10 μM) for 0–120 min. (**B**–**D**) DNA binding activities of AP-1 family of proteins (B) Fos (cFos, FosB), (C) Jun (JunB, cJun, JunD), and (D) Fra-1 in nuclear proteins extracts from cells treated with PGE$_2$ (10 μM) for 60 min. Data are mean ± SD (n = 3). *$p < 0.05$, **$p < 0.01$ (compared with control).

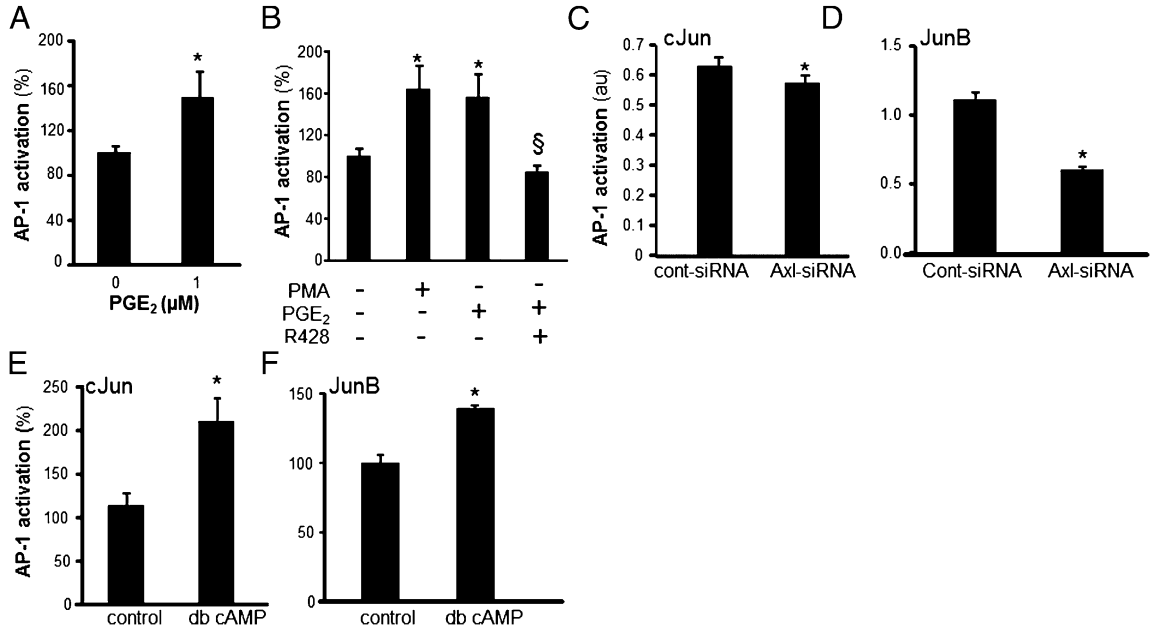

FIGURE 7. cAMP and Axl regulate cJun and JunB DNA binding activities. (**A**) DNA binding activity of AP-1 in THP-1 differentiated mϕ treated with PGE_2 (1 μM) for 60 min. Data are mean ± SD ($n = 3$). *$p < 0.05$ (compared with control). (**B**) Cells were pretreated (1 h) with R428 (Axl inhibitor, SYN-1131, 1 μM) followed by activation with PGE_2 (10 μM, 1 h). DNA binding activity of AP-1 was determined. PMA (1 μM, 1 h) was used as a classical inducer of AP-1 activity to compare the extent of PGE_2-induced AP-1 activation. Data are mean ± SD ($n = 3$). *$p < 0.05$ (compared with control). (**C** and **D**) Axl knockdown in differentiated human THP-1 mϕ (Axl-siRNA) or control (cont-siRNA) were treated with PGE_2 for 1 h. (C) cJun and (D) JunB DNA binding activities were determined from nuclear proteins using Trans-AM assay. Data are mean ± SD ($n = 3$). *$p < 0.05$ (compared with controls). (**E** and **F**) Cells were treated with db-cAMP (100 μM, 1 h). (E) cJun and (F) JunB DNA binding activities were determined from nuclear proteins using Trans-AM assay. Data are mean ± SD ($n = 3$). *$p < 0.05$ (compared with control).

uation of OSM mRNA expression in murine wound mϕ as well as attenuated level of PGE_2 in wound fluid suggesting that endogenous cyclooxygenase-derived PGs are involved in inducing OSM in wound macrophages (Fig. 9E, 9F).

To elucidate the significance of OSM on the inflammatory properties of mϕ, human mϕ were treated with human recombinant OSM. The response of human mϕ to OSM in a setting of LPS-induced inflammation was evaluated using a multiplex cytokine array approach (Fig. 10A). OSM clearly modified the inflammatory response of LPS-treated mϕ. Of note, a decline in LPS-induced expression of proinflammatory cytokines, TNF-α and IL-1β, was observed. This array finding was verified independently using ELISA supporting plausible anti-inflammatory properties of OSM (Fig. 10B). To test the significance of OSM in wound inflammation in vivo, murine excisional wounds were investigated. Treatment of such wounds with recombinant murine OSM during the early inflammatory phase resulted in increased abundance of tissue OSM in treated wounds demonstrating successful delivery of OSM (Fig. 10C). Such treatment proved to be anti-inflammatory by suppressing the expression of proinflammatory cytokines TNF-α and IL-1β (Fig. 10D). OSM-treated wounds also showed improved closure outcomes at day 3 (Fig. 10E).

Discussion

The chronic wound microenvironment featuring lower pH, high proteolytic activity, high abundance of lactate, and often hosting infection is generally nonconducive to healing (34). Dynamic reciprocity, as an ongoing, bidirectional interaction among cells and their surrounding microenvironment, is viewed as a key contributor to wound healing wherein biochemical, biophysical, and cellular responses to injury play pivotal roles in regulating healing responses to injury (35). Monocyte and mϕ functions are highly responsive to their microenvironment. Although this is well characterized in the context of cancer biology (36, 37), there is a void of information on how the human chronic wound microenvironment modifies wound mϕ biology. Current understanding of chronic wound inflammation is primarily based on information from MDM originating from peripheral blood. These cells have never been exposed to the wound microenvironment and therefore are unlikely to be primed by such conditions. Indeed, changes in mϕ phenotype associated with the progression of wound healing do not follow the current mϕ classifications (6, 7). The need to understand unique characteristics of wound mϕ are therefore compelling and would help elucidate novel pathways implicated in determining wound inflammation outcomes.

OSM is an IL-6 family protein discovered in the supernatant of human monocytic cells in 1986 and known to be produced by activated mϕ (9). The anti-inflammatory properties of mϕ-derived OSM are currently unfolding (38). Although the beneficial properties of OSM against cancer is documented (39), to our knowledge this work presents the first evidence demonstrating a novel role of OSM as an anti-inflammatory molecule that is abundantly produced by wound mϕ. High levels of OSM have been reported in several unrelated inflammatory scenarios (40, 41). This work reports an abundance of OSM in wound fluid. OSM expression in mϕ is known to be induced by factors relevant to the wound site such as pathogenic bacteria (42), blood coagulation factors such as thrombin (43), and complement component C5a (44). Among lipid mediators, PGE_2 is recognized as a potent inducer of OSM expression (24). PGs are lipid autocoids derived from arachidonic acid. They both sustain homeostatic functions and mediate pathogenic mechanisms, including the inflammatory response (45). PGE_2 is the most abundant eicosanoid (lipid mediators generated through oxidative pathways from arachidonic acid). Anti-inflammatory properties of PGE_2 are currently unfolding in the context of tumor biology (46). PGE_2 helps resolve inflam-

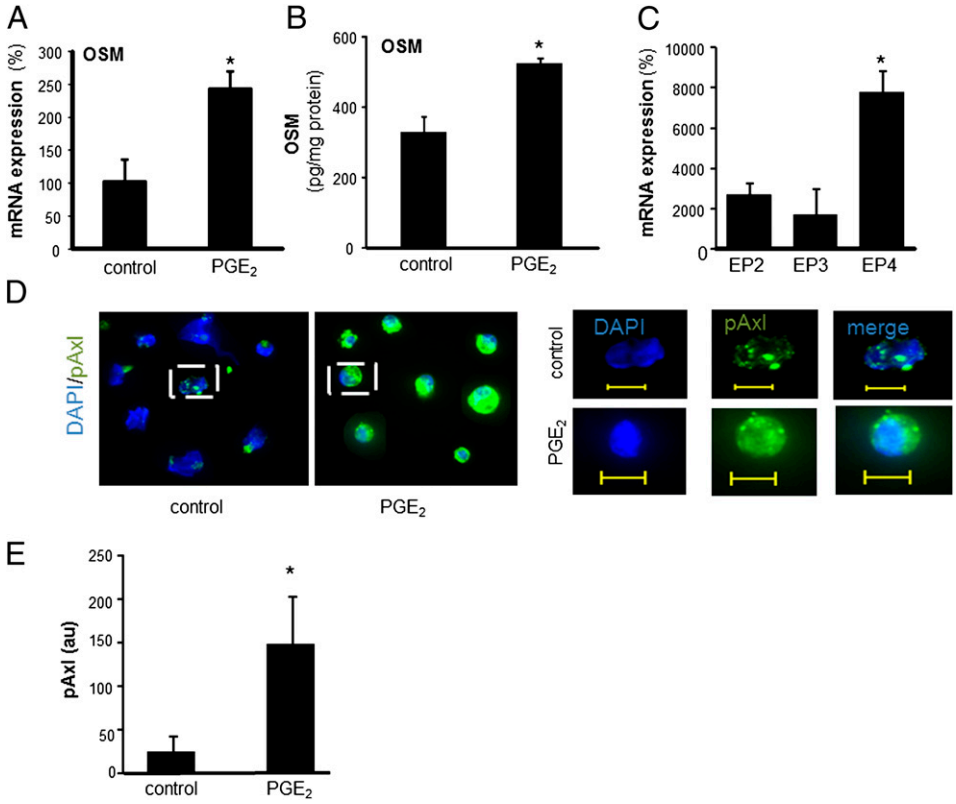

FIGURE 8. PGE$_2$-mediated induction of OSM and pAxl in human and mice wound mϕ. (**A**) PVA sponges containing 20 μl 0.1 mM PGE$_2$ (2 nmol/sponge) or ethanol (matching volume, 20 μl) were implanted s.c. at the back of mice. Wound mϕ were harvested 3 d postimplantation, and OSM mRNA expression was determined using qPCR. Data are mean ± SD (n = 3) *$p < 0.05$ (compared with control). (**B**) The mϕ from human chronic wounds were isolated and treated with PGE$_2$ (10 μM, 24 h). Controls were treated with matching volume of ethanol. OSM levels in culture media of wound mϕ were measured using ELISA. Data were normalized to total protein levels. Data are mean ± SD (n = 3). *$p < 0.05$ (compared with control). (**C**) Relative expression of EP receptors in human wound mϕ. mRNA expression of EP receptors was determined using qPCR. Data are mean ± SD (n = 4). *$p < 0.01$ (compared with EP2–EP3). (**D**) Human wound mϕ were stained with anti-pAxl Ab (green) and DAPI (blue nucleus). Increased expression of pAxl in wound mϕ treated with PGE$_2$ (10 μM, 30 min) can be seen. *Left*, Low-magnification images. *Right*, High-magnification images of the cell marked in the respective *left panel*. Scale bar, 10 μM. (**E**) Quantification of the fluorescence signal shown in (D) using Axiovision (Zeiss). *$p < 0.05$ (compared with control).

mation by targeting the NF-κB pathway (47). Indeed, administration of esterified PGE$_2$ during the early phase of wound healing showed anti-inflammatory outcomes (48). Abundance of PGE$_2$ at the wound site has been previously reported (49, 50), and findings of the current study support such observations by reporting high levels of PGE$_2$ in the wound fluid. Part of this PGE$_2$ in the wound microenvironment is contributed by wound mϕ. The findings of this study extend that observation to establish a cause and effect relationship between PGE$_2$ at the wound site and induction of OSM in wound mϕ. OSM levels in mϕ derived from human chronic wounds as well as from acute murine wounds were elevated in response to PGE$_2$ treatment. That PGE$_2$ may induce anti-inflammatory responses in mϕ by inhibiting adhesion molecule expression is already reported (51). The current work unequivocally demonstrates that at the wound site accumulated PGE$_2$ induces OSM, which supports wound healing via anti-inflammatory pathways. PGE$_2$ is known to induce OSM expression in microglia, monocytes, and mϕ of human and murine origin via G-protein–coupled receptors cAMP and protein kinase A (24). PGE$_2$ biosynthesis is noted to have a central role in skin repair. Topically administered PGE$_2$ (dinoprostone) restored normal wound repair. However, the mechanisms underlying the effects of PGE$_2$ on adult dermal wound healing remain unclear. The current study recognizes that PGE$_2$ is a potent inducer of OSM expression in mϕ derived from human chronic wounds.

Secreted PGE$_2$ acts in an autocrine or paracrine manner through its four cognate G-protein–coupled receptors EP1 to EP4 (52). Mϕ predominantly express EP2 and EP4 receptors that are coupled to G-proteins and signal by stimulating adenylyl cyclase (53). That PGE$_2$-mediated OSM expression involves cAMP signaling has been directly demonstrated in microglial cells as well as in human mϕ (24). The current work provides the first evidence to our knowledge directly implicating RTK in PGE$_2$-induced signaling directed at OSM expression. Specifically, the findings of the study recognized RTK Axl to be phosphorylated in response to PGE$_2$ treatment. Despite 90% knockdown of Axl levels in cells, a modest (~40%) decrease in the level of OSM was noted. Such an effect may be because of the fact that residual Axl function following Axl knockdown is sufficient to transduce signals toward OSM expression. Long turnover time for preexisting OSM protein could be a contributing factor as well. Axl receptors are known to serve anti-inflammatory functions by suppressing inflammatory cytokine production (54). Also, loss of Axl results in enhanced inflammatory response (55). A striking general observation of the current study is the cross talk between RTK and cAMP signaling cascades. Exposure of cells to a cAMP analogue led to Axl phosphorylation. Both pathways, RTK as well as cAMP, contributed to PGE$_2$-induced expression OSM.

Axl (also called UFO, ARK, and Tyro7) RTKs are expressed at abnormally high levels in a variety of malignancies and support

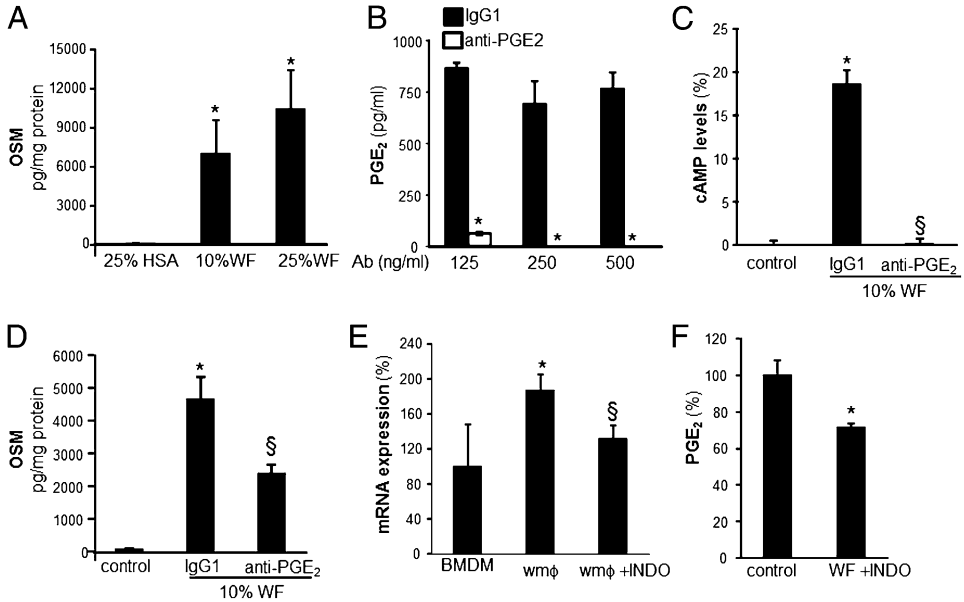

FIGURE 9. Wound fluid PGE_2 and cyclooxygenase-derived PG induced OSM in human and murine wound mϕ. (**A**) Human MDM were treated with varying dilutions (0–25%, v/v, 72 h) of wound fluid (WF) derived from human chronic wounds. WF was sterile filtered and added directly to the MDM culture medium. For control, a matching volume of human AB serum (HSA) was added to the culture medium. OSM levels were measured in culture media 72 h after treatment with WF. Data are mean ± SD ($n = 4$). *$p < 0.05$ (compared with control). (**B**) To determine the dose of anti-PGE_2 Ab (Ab, clone 2B5) that may effectively sequester PGE_2 from WF, varying (125–500 ng/ml) concentrations of anti-PGE_2 Ab or equivalent amount of IgG1 was added to the WF. PGE_2 level in WF was determined using ELISA. Data are mean ± SD ($n = 4$). *$p < 0.05$ (compared with control). (**C** and **D**) WF (10% v/v) was pretreated with anti-PGE_2 or corresponding IgG1 (250 ng/ml) to sequester PGE_2 followed by treatment of MDM with WF (10% v/v) for 72 h. (C) cAMP level in culture media was determined using ELISA. Data are mean ± SD ($n = 3$). *$p < 0.05$ (compared with control). (D) OSM level in culture medium was determined using ELISA. Data are mean ± SD ($n = 3$). *$p < 0.05$ (compared with control). (**E** and **F**) Mice (C57Bl/6, 9 wk old) were supplemented (intragastric) with indomethacin (INDO, 1 mg/kg/day) or vehicle (saline) for 5 consecutive days. PVA sponges or Hunt–Schilling wire mesh cylinders were s.c. implanted in the backs of mice on the third day after supplementation. Wound mϕ (PVA sponges) and wound fluid (WF, wire mesh cylinders) were harvested 3 d postimplantation, and (E) OSM mRNA expression (mϕ) or (F) PGE_2 level in WF was determined using qPCR or ELISA, respectively. BMDM were obtained from INDO untreated mice. Data are mean ± SD ($n = 3$). *$p < 0.05$ (compared with BMDM), §$p < 0.05$ (compared with wound mϕ).

mitogenesis. Axl is activated by autophosphorylation (56). The mitogenic transcription factor AP-1 is known to promote Axl expression (57, 58). Observations reported in this study provide the first evidence to our knowledge that Axl supports AP-1 transactivation. Given the key role of AP-1 in executing mitogenesis and an established function of Axl in promoting tumor growth, it is understandable that Axl engages AP-1 for downstream signaling. AP-1 complexes are composed of members of the Jun (cJun, JunB, JunD), and Fos (cFos, FosB, Fra-1, and Fra-2) families and bind to specific control elements present in the promoters of genes that regulate cell differentiation and proliferation (59). Members of the Fos family heterodimerize with Jun family members, thus forming the AP-1 complex, which transcriptionally regulates numerous genes (59). The findings of this study reveal that members of the Jun family, specifically cJun and JunB but not JunD, were induced by PGE_2 treatment. The observation that PGE_2 may induce Jun proteins is consistent with a previous observation reported in bone-derived fibroblasts (60). Both cJun and JunB contain functional JNK docking sites whereas JunD lacks such sites (61) suggesting a likely involvement of JNK in the Axl-induced cJun and JunB activation pathway.

OSM is a late-phase cytokine that elicits an anti-inflammatory response by altering the activities of initiators of the inflammatory response (62). Treatment with OSM attenuated the severity of LPS-induced joint inflammation (62). The biological functions of OSM are executed through binding of the cytokine to specific OSM receptor subunit β (8). In OSM receptor subunit β-deficient mice, peritoneal inflammation is associated with enhanced recruitment of monocytic cells suggesting an anti-inflammatory role of OSM signaling in limiting of monocyte recruitment (63). Production of OSM during the early wound inflammatory phase has been linked to PMN (8). The role of mϕ as an inducible source of OSM in the wound milieu as well as the significance of OSM in wound healing remained unknown. This work address both gaps, providing a mechanism for how OSM is induced at the wound site. Furthermore, the findings of the current study support that when made available during the early phase of wound healing, OSM elicits an anti-inflammatory response by suppressing the expression of proinflammatory cytokines TNF-α and IL-1β by wound-site mϕ. Such anti-inflammatory property of OSM is in accordance with previous reports demonstrating in vivo anti-inflammatory effects of OSM (62).

The wound habitat is isolated and distinguished from its immediate surrounding tissue. The wound fluid bathing the wound tissue reflects the wound microenvironment and shapes the functional response of wound-related cells (64). The approach to study mϕ, differentiated from peripheral blood monocytes in a laboratory setting, is limited in its ability to account for interactions between the wound microenvironment and wound-resident mϕ. This work provides to our knowledge the first evidence from a direct pair-matched comparison of the MDM versus wound mϕ that identifies OSM as a protein differentially overexpressed in wound mϕ. PGE_2, recognized as a growth-promoting autocoid for epidermis, is known to be synthesized in excess at the site of wound healing (65). This work demonstrated that wound-site PGE_2 induces OSM in wound mϕ via a pathway that involves both

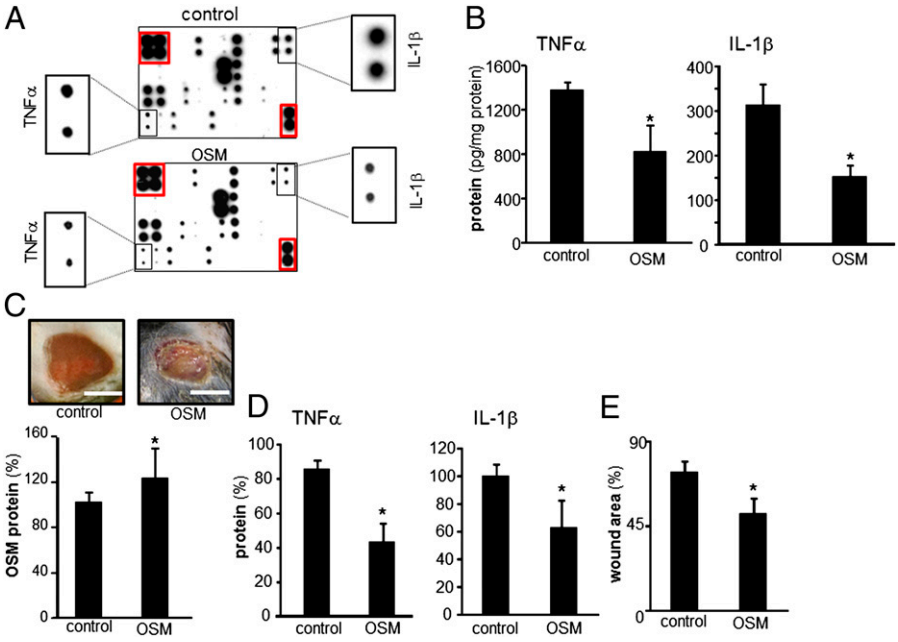

FIGURE 10. Anti-inflammatory activity of OSM in macrophages and wound inflammation. (A and B) Human mϕ treated with OSM (25 ng/ml, 72 h) followed by treatment with LPS (1 μg/ml, 24 h). (**A**) A multiplex cytokine array was performed to evaluate the effect of OSM on LPS-induced inflammatory response in human mϕ. The spots marked with red line are housekeeping controls. The zoom of the respective spots for IL-1β and TNF-α from each array are shown as insets. (**B**) The levels of LPS-induced TNF-α and IL-1β in OSM pretreated mϕ was independently measured using ELISA. Data are mean ± SD ($n = 3$). *$p < 0.05$ (compared with control). (**C**–**E**) Effect of OSM on wound inflammation was evaluated using a murine excisional wound model. (C) Representative day 3 post-wounding images from excisional wounds treated with recombinant mouse OSM (1.25 μg/15 μl/wound) in early inflammatory phase (0–3 d post-wounding). Control wounds received vehicle only. OSM levels on day 3 post-wounding in wound tissue treated with recombinant OSM. (D) TNF-α and IL-1β in OSM-pretreated excisional wound on day 3 post-wounding. Data are mean ± SD ($n = 3$) *$p < 0.05$ (compared with control). (E) Wound area in OSM-pretreated excisional wound on day 3 post-wounding. Wound area is presented as percentage compared with wound size at day 0 post-wounding. Data are mean ± SD ($n = 3$). *$p < 0.05$ (compared with control).

cAMP and RTK signaling. Finally, the observation that OSM functions as an anti-inflammatory agent at the wound site introduces a novel element in the overall biology addressing the control of wound inflammation.

Disclosures

The authors have no financial conflicts of interest.

References

1. Sen, C. K., G. M. Gordillo, S. Roy, R. Kirsner, L. Lambert, T. K. Hunt, F. Gottrup, G. C. Gurtner, and M. T. Longaker. 2009. Human skin wounds: a major and snowballing threat to public health and the economy. *Wound Repair Regen.* 17: 763–771.
2. Leibovich, S. J., and R. Ross. 1975. The role of the macrophage in wound repair. A study with hydrocortisone and antimacrophage serum. *Am. J. Pathol.* 78: 71–100.
3. Lucas, T., A. Waisman, R. Ranjan, J. Roes, T. Krieg, W. Müller, A. Roers, and S. A. Eming. 2010. Differential roles of macrophages in diverse phases of skin repair. *J. Immunol.* 184: 3964–3977.
4. Geissmann, F., M. G. Manz, S. Jung, M. H. Sieweke, M. Merad, and K. Ley. 2010. Development of monocytes, macrophages, and dendritic cells. *Science* 327: 656–661.
5. Stout, R. D., and J. Suttles. 2004. Functional plasticity of macrophages: reversible adaptation to changing microenvironments. *J. Leukoc. Biol.* 76: 509–513.
6. Daley, J. M., S. K. Brancato, A. A. Thomay, J. S. Reichner, and J. E. Albina. 2010. The phenotype of murine wound macrophages. *J. Leukoc. Biol.* 87: 59–67.
7. Brancato, S. K., and J. E. Albina. 2011. Wound macrophages as key regulators of repair: origin, phenotype, and function. *Am. J. Pathol.* 178: 19–25.
8. Goren, I., H. Kämpfer, E. Müller, D. Schiefelbein, J. Pfeilschifter, and S. Frank. 2006. Oncostatin M expression is functionally connected to neutrophils in the early inflammatory phase of skin repair: implications for normal and diabetes-impaired wounds. *J. Invest. Dermatol.* 126: 628–637.
9. Tanaka, M., and A. Miyajima. 2003. Oncostatin M, a multifunctional cytokine. *Rev. Physiol. Biochem. Pharmacol.* 149: 39–52.
10. Gómez-Lechón, M. J. 1999. Oncostatin M: signal transduction and biological activity. *Life Sci.* 65: 2019–2030.
11. Roy, S., R. Dickerson, S. Khanna, E. Collard, U. Gnyawali, G. M. Gordillo, and C. K. Sen. 2011. Particulate β-glucan induces TNF-α production in wound macrophages via a redox-sensitive NF-κβ-dependent pathway. *Wound Repair Regen.* 19: 411–419.
12. Khanna, S., S. Biswas, Y. Shang, E. Collard, A. Azad, C. Kauh, V. Bhasker, G. M. Gordillo, C. K. Sen, and S. Roy. 2010. Macrophage dysfunction impairs resolution of inflammation in the wounds of diabetic mice. *PLoS ONE* 5: e9539.
13. Vairo, G., and J. A. Hamilton. 1985. CSF-1 stimulates Na+K+-ATPase mediated 86Rb+ uptake in mouse bone marrow-derived macrophages. *Biochem. Biophys. Res. Commun.* 132: 430–437.
14. Davies, J. Q., and S. Gordon. 2005. Isolation and culture of murine macrophages. In *Basic Cell Culture Protocols.* C. D. Helgason, and C. L. Miller, eds. Humana Press, Totowa, NJ, p. 91–103.
15. Roy, S., S. Khanna, K. Nallu, T. K. Hunt, and C. K. Sen. 2006. Dermal wound healing is subject to redox control. *Mol. Ther.* 13: 211–220.
16. Galiano, R. D., J. Michaels, V, M. Dobryansky, J. P. Levine, and G. C. Gurtner. 2004. Quantitative and reproducible murine model of excisional wound healing. *Wound Repair Regen.* 12: 485–492.
17. Roy, S., S. Khanna, C. Rink, S. Biswas, and C. K. Sen. 2008. Characterization of the acute temporal changes in excisional murine cutaneous wound inflammation by screening of the wound-edge transcriptome. *Physiol. Genomics* 34: 162–184.
18. Roy, S., S. Khanna, D. E. Kuhn, C. Rink, W. T. Williams, J. L. Zweier, and C. K. Sen. 2006. Transcriptome analysis of the ischemia-reperfused remodeling myocardium: temporal changes in inflammation and extracellular matrix. *Physiol. Genomics* 25: 364–374.
19. Roy, S., S. Khanna, P. E. Yeh, C. Rink, W. B. Malarkey, J. Kiecolt-Glaser, B. Laskowski, R. Glaser, and C. K. Sen. 2005. Wound site neutrophil transcriptome in response to psychological stress in young men. *Gene Expr.* 12: 273–287.
20. Roy, S., D. Patel, S. Khanna, G. M. Gordillo, S. Biswas, A. Friedman, and C. K. Sen. 2007. Transcriptome-wide analysis of blood vessels laser captured from human skin and chronic wound-edge tissue. *Proc. Natl. Acad. Sci. USA* 104: 14472–14477.
21. Roy, S., S. Khanna, W. A. Wallace, J. Lappalainen, C. Rink, A. J. Cardounel, J. L. Zweier, and C. K. Sen. 2003. Characterization of perceived hyperoxia in isolated primary cardiac fibroblasts and in the reoxygenated heart. *J. Biol. Chem.* 278: 47129–47135.
22. Verducci, J. S., V. F. Melfi, S. Lin, Z. Wang, S. Roy, and C. K. Sen. 2006. Microarray analysis of gene expression: considerations in data mining and statistical treatment. *Physiol. Genomics* 25: 355–363.
23. Roy, S., S. Khanna, A. Azad, R. Schnitt, G. He, C. Weigert, H. Ichijo, and C. K. Sen. 2010. Fra-2 mediates oxygen-sensitive induction of transforming growth factor beta in cardiac fibroblasts. *Cardiovasc. Res.* 87: 647–655.
24. Repovic, P., and E. N. Benveniste. 2002. Prostaglandin E2 is a novel inducer of oncostatin-M expression in macrophages and microglia. *J. Neurosci.* 22: 5334–5343.

25. Hamberg, M., and B. Samuelsson. 1971. On the metabolism of prostaglandins E 1 and E 2 in man. *J. Biol. Chem.* 246: 6713–6721.
26. Repovic, P., K. Mi, and E. N. Benveniste. 2003. Oncostatin M enhances the expression of prostaglandin E2 and cyclooxygenase-2 in astrocytes: synergy with interleukin-1beta, tumor necrosis factor-alpha, and bacterial lipopolysaccharide. *Glia* 42: 433–446.
27. Stenson, W. F., and C. W. Parker. 1980. Prostaglandins, macrophages, and immunity. *J. Immunol.* 125: 1–5.
28. Ushikubi, F., M. Hirata, and S. Narumiya. 1995. Molecular biology of prostanoid receptors; an overview. *J. Lipid Mediat. Cell Signal.* 12: 343–359.
29. Cherukuri, D. P., X. B. Chen, A. C. Goulet, R. N. Young, Y. Han, R. L. Heimark, J. W. Regan, E. Meuillet, and M. A. Nelson. 2007. The EP4 receptor antagonist, L-161,982, blocks prostaglandin E2-induced signal transduction and cell proliferation in HCA-7 colon cancer cells. *Exp. Cell Res.* 313: 2969–2979.
30. Regan, J. W. 2003. EP2 and EP4 prostanoid receptor signaling. *Life Sci.* 74: 143–153.
31. Ma, Y., R. J. Streiff, J. Liu, M. J. Spence, and R. E. Vestal. 1999. Cloning and characterization of human oncostatin M promoter. *Nucleic Acids Res.* 27: 4649–4657.
32. Mollinedo, F., C. Gajate, A. Tugores, I. Flores, and J. R. Naranjo. 1993. Differences in expression of transcription factor AP-1 in human promyelocytic HL-60 cells during differentiation towards macrophages versus granulocytes. *Biochem. J.* 294: 137–144.
33. Holland, S. J., A. Pan, C. Franci, Y. Hu, B. Chang, W. Li, M. Duan, A. Torneros, J. Yu, T. J. Heckrodt, et al. 2010. R428, a selective small molecule inhibitor of Axl kinase, blocks tumor spread and prolongs survival in models of metastatic breast cancer. *Cancer Res.* 70: 1544–1554.
34. Falanga, V. 1992. Growth factors and chronic wounds: the need to understand the microenvironment. *J. Dermatol.* 19: 667–672.
35. Schultz, G. S., J. M. Davidson, R. S. Kirsner, P. Bornstein, and I. M. Herman. 2011. Dynamic reciprocity in the wound microenvironment. *Wound Repair Regen.* 19: 134–148.
36. Moussai, D., H. Mitsui, J. S. Pettersen, K. C. Pierson, K. R. Shah, M. Suárez-Fariñas, I. R. Cardinale, M. J. Bluth, J. G. Krueger, and J. A. Carucci. 2011. The human cutaneous squamous cell carcinoma microenvironment is characterized by increased lymphatic density and enhanced expression of macrophage-derived VEGF-C. *J. Invest. Dermatol.* 131: 229–236.
37. Stearman, R. S., L. Dwyer-Nield, M. C. Grady, A. M. Malkinson, and M. W. Geraci. 2008. A macrophage gene expression signature defines a field effect in the lung tumor microenvironment. *Cancer Res.* 68: 34–43.
38. Dumas, A., S. Lagarde, C. Laflamme, and M. Pouliot. 2012. Oncostatin M decreases interleukin-1 β secretion by human synovial fibroblasts and attenuates an acute inflammatory reaction in vivo. *J. Cell. Mol. Med.* 16: 1274–1285.
39. David, E., P. Guihard, B. Brounais, A. Riet, C. Charrier, S. Battaglia, F. Gouin, S. Ponsolle, R. L. Bot, C. D. Richards, et al. 2011. Direct anti-cancer effect of oncostatin M on chondrosarcoma. *Int. J. Cancer* 128: 1822–1835.
40. Huang, F. M., C. H. Tsai, S. F. Yang, and Y. C. Chang. 2009. The upregulation of oncostatin M in inflamed human dental pulps. *Int. Endod. J.* 42: 627–631.
41. Albasanz-Puig, A., J. Murray, M. Preusch, D. Coan, M. Namekata, Y. Patel, Z. M. Dong, M. E. Rosenfeld, and E. S. Wijelath. 2011. Oncostatin M is expressed in atherosclerotic lesions: a role for Oncostatin M in the pathogenesis of atherosclerosis. *Atherosclerosis* 216: 292–298.
42. Zeaiter, Z., H. Diaz, M. Stein, and H. Q. Huynh. 2011. *Helicobacter pylori* induces expression and secretion of oncostatin M in macrophages in vitro. *Dig. Dis. Sci.* 56: 689–697.
43. Kastl, S. P., W. S. Speidl, K. M. Katsaros, C. Kaun, G. Rega, A. Assadian, G. W. Hagmueller, M. Hoeth, R. de Martin, Y. Ma, et al. 2009. Thrombin induces the expression of oncostatin M via AP-1 activation in human macrophages: a link between coagulation and inflammation. *Blood* 114: 2812–2818.
44. Kastl, S. P., W. S. Speidl, C. Kaun, K. M. Katsaros, G. Rega, T. Afonyushkin, V. N. Bochkov, P. Valent, A. Assadian, G. W. Hagmueller, et al. 2008. In human macrophages the complement component C5a induces the expression of oncostatin M via AP-1 activation. *Arterioscler. Thromb. Vasc. Biol.* 28: 498–503.
45. Ricciotti, E., and G. A. FitzGerald. 2011. Prostaglandins and inflammation. *Arterioscler. Thromb. Vasc. Biol.* 31: 986–1000.
46. Van Elssen, C. H., J. Vanderlocht, T. Oth, B. L. Senden-Gijsbers, W. T. Germeraad, and G. M. Bos. 2011. Inflammation-restraining effects of prostaglandin E2 on natural killer-dendritic cell (NK-DC) interaction are imprinted during DC maturation. *Blood* 118: 2473–2482.
47. Gomez, P. F., M. H. Pillinger, M. Attur, N. Marjanovic, M. Dave, J. Park, C. O. Bingham, III, H. Al-Mussawir, and S. B. Abramson. 2005. Resolution of inflammation: prostaglandin E2 dissociates nuclear trafficking of individual NF-kappaB subunits (p65, p50) in stimulated rheumatoid synovial fibroblasts. *J. Immunol.* 175: 6924–6930.
48. Talwar, M., T. N. Moyana, B. Bharadwaj, and L. K. Tan. 1996. The effect of a synthetic analogue of prostaglandin E2 on wound healing in rats. *Ann. Clin. Lab. Sci.* 26: 451–457.
49. Baxter, C. R. 1994. Immunologic reactions in chronic wounds. *Am. J. Surg.* 167 (1A): 12S–14S.
50. Egg, D. 1984. Concentrations of prostaglandins D2, E2, F2 alpha, 6-keto-F1 alpha and thromboxane B2 in synovial fluid from patients with inflammatory joint disorders and osteoarthritis. *Z. Rheumatol.* 43: 89–96.
51. Hasegawa, S., T. Ichiyama, F. Kohno, Y. Korenaga, A. Ohsaki, R. Hirano, Y. Haneda, R. Fukano, and S. Furukawa. 2010. Prostaglandin E2 suppresses beta1-integrin expression via E-prostanoid receptor in human monocytes/macrophages. *Cell. Immunol.* 263: 161–165.
52. Suzawa, T., C. Miyaura, M. Inada, T. Maruyama, Y. Sugimoto, F. Ushikubi, A. Ichikawa, S. Narumiya, and T. Suda. 2000. The role of prostaglandin E receptor subtypes (EP1, EP2, EP3, and EP4) in bone resorption: an analysis using specific agonists for the respective EPs. *Endocrinology* 141: 1554–1559.
53. Nataraj, C., D. W. Thomas, S. L. Tilley, M. T. Nguyen, R. Mannon, B. H. Koller, and T. M. Coffman. 2001. Receptors for prostaglandin E(2) that regulate cellular immune responses in the mouse. *J. Clin. Invest.* 108: 1229–1235.
54. Sharif, M. N., D. Sosic, C. V. Rothlin, E. Kelly, G. Lemke, E. N. Olson, and L. B. Ivashkiv. 2006. Twist mediates suppression of inflammation by type I IFNs and Axl. *J. Exp. Med.* 203: 1891–1901.
55. Weinger, J. G., C. F. Brosnan, O. Loudig, M. F. Goldberg, F. Macian, H. A. Arnett, A. L. Prieto, V. Tsiperson, and B. Shafit-Zagardo. 2011. Loss of the receptor tyrosine kinase Axl leads to enhanced inflammation in the CNS and delayed removal of myelin debris during experimental autoimmune encephalomyelitis. *J. Neuroinflammation* 8: 49.
56. Konishi, A., T. Aizawa, A. Mohan, V. A. Korshunov, and B. C. Berk. 2004. Hydrogen peroxide activates the Gas6-Axl pathway in vascular smooth muscle cells. *J. Biol. Chem.* 279: 28766–28770.
57. Mudduluru, G., J. H. Leupold, P. Stroebel, and H. Allgayer. 2010. PMA up-regulates the transcription of Axl by AP-1 transcription factor binding to TRE sequences via the MAPK cascade in leukaemia cells. *Biol. Cell* 103: 21–33.
58. Sayan, A. E., R. Stanford, R. Vickery, E. Grigorenko, J. Diesch, K. Kulbicki, R. Edwards, R. Pal, P. Greaves, I. Jariel-Encontre, et al. 2012. Fra-1 controls motility of bladder cancer cells via transcriptional upregulation of the receptor tyrosine kinase AXL. *Oncogene* 31: 1493–1503.
59. Hess, J., P. Angel, and M. Schorpp-Kistner. 2004. AP-1 subunits: quarrel and harmony among siblings. *J. Cell Sci.* 117: 5965–5973.
60. Suda, M., K. Tanaka, Y. Sakuma, A. Yasoda, A. Ozasa, J. Fukata, I. Tanaka, S. Narumiya, and K. Nakao. 2000. Prostaglandin E(2) (PGE(2)) induces the c-fos and c-jun expressions via the EP(1) subtype of PGE receptor in mouse osteoblastic MC3T3-E1 cells. *Calcif. Tissue Int.* 66: 217–223.
61. Mechta-Grigoriou, F., D. Gerald, and M. Yaniv. 2001. The mammalian Jun proteins: redundancy and specificity. *Oncogene* 20: 2378–2389.
62. Wahl, A. F., and P. M. Wallace. 2001. Oncostatin M in the anti-inflammatory response. *Ann. Rheum. Dis.* 60(Suppl 3): iii75–iii80.
63. Hams, E., C. S. Colmont, V. Dioszeghy, V. J. Hammond, C. A. Fielding, A. S. Williams, M. Tanaka, A. Miyajima, P. R. Taylor, N. Topley, and S. A. Jones. 2008. Oncostatin M receptor-beta signaling limits monocytic cell recruitment in acute inflammation. *J. Immunol.* 181: 2174–2180.
64. Drinkwater, S. L., A. Smith, and K. G. Burnand. 2002. What can wound fluids tell us about the venous ulcer microenvironment? *Int. J. Low. Extrem. Wounds* 1: 184–190.
65. Pentland, A. P., and P. Needleman. 1986. Modulation of keratinocyte proliferation in vitro by endogenous prostaglandin synthesis. *J. Clin. Invest.* 77: 246–251.